

Transport mechanism and paleoclimatic significance of terrigenous silt deposited in varved sediments of an African rift lake

Thomas C. Johnson

Large Lakes Observatory and Department of Geological Sciences, University of Minnesota Duluth, Duluth, Minnesota 55812

I. N. McCave

Department of Earth Sciences, University of Cambridge, Downing Street, Cambridge, United Kingdom CB2 3EQ

Abstract

We analyzed a varved sequence of sediment from a 350-m depth in the north basin of Lake Malawi, East Africa, for the size distribution of the sortable silt fraction (10–64 μm). Mean size of the sortable silt (\overline{SS}) varies measurably in sediments spanning the past 650 yr and covaries with the mass accumulation rate of terrigenous silt and clay ($TMAR$) over much of the interval. Most of the silt and clay is delivered to the offshore basin in benthic nepheloid plumes of unknown duration and frequency. $TMAR$ appears to be related to annual rainfall (which is related to the North Atlantic Oscillation) because it roughly tracks the historical record of lake level that extends back to 1860. \overline{SS} should be related to density or thickness of underflow, thus related to resuspension intensity or river flood loading. It also tracks lake level and regional wind strength as determined by National Center for Environmental Prediction (NCEP) Reanalysis.

The distribution of sediment sizes in lake basins is strongly bimodal; relatively coarse sand and gravel accumulate in the shallower depths where the oscillatory flow due to surface waves winnows away the fine-grained material and silty clay accumulates at greater depths, below the “mud-depositional boundary” (Rowan et al. 1992; Hakanson and Kallstrom 1978). The deep basins of the East African rift lakes, which can be several hundred meters deep and tens of kilometers across, provide immense repositories of organically rich mud up to several kilometers thick. The mud-depositional boundary is ~ 100 m in the large lakes of Tanganyika and Malawi, and ~ 30 m to 40 m in the smaller lakes such as Edward and Albert (Johnson 1996; cf. the “mud line” of the U.S. mid-Atlantic Bight slope at 250–300 m [Stanley and Wear 1978]). The mud is typically diatomaceous silty clay, usually deposited under anoxic conditions, with 5–30 wt% of organic carbon (Talbot 1988).

Here we examine the accumulation rate of terrigenous clastic sediment and the size distribution of “sortable silt” in the north basin mud of Lake Malawi. Sortable silt (SS) is defined by a size range of 10 μm to 63 μm and has been argued to respond in a dominantly noncohesive manner that is particularly sensitive to bottom-current strength

(McCave and Hall 2006; McCave et al. 2006). Fluctuations in the mean size of the SS (\overline{SS}) have been found to reflect changes in ocean-bottom current intensity; vigorous flow inhibits the deposition of the slower settling (finer-grained) sediment. This results in a relatively coarse \overline{SS} as well as a high percentage of SS (SS%) in the fine-grained deposits.

Given the proximity of the shoreline and large rivers to the northern basin of Lake Malawi, the problem considered here is how the accumulating sediment is delivered: from direct fluvial input, aeolian fallout, or resuspension and dispersal in midwater or bottom plumes. We analyzed a sediment record spanning the past 650 yr, addressing both the mechanism by which the SS is transported to the offshore basin and the paleoclimatic significance of \overline{SS} variability through time.

Methods

Piston cores and multicores were recovered from five sites in 250–450-m water depth in the north basin in 1998 (Barry et al. 2002). We selected multicore M98-11MC and nearby gravity pilot core M98-2PG from depths of 363 m and 404 m, respectively, for this study (Fig. 1). The sediment is laminated, diatomaceous silty clay, with alternating light laminae rich in diatom frustules and dark laminae with high concentrations of terrigenous silty clay. A comparison of lamination counts and Pb-210 analyses demonstrated that these laminations are annual layers, or varves, with the light, diatomaceous laminae interpreted to reflect the dry, windy months of austral winter, when upwelling promotes high algal productivity, and the dark, clastic laminations interpreted to correspond to the rainy months of austral summer, when river discharge is at a maximum (Pilskaln and Johnson 1991; Johnson et al. 2001). An age model was established previously for these cores, based on (1) Pb-210 dates for the past 100 yr in core

Acknowledgments

TCJ thanks St. John's College, University of Cambridge, for providing an Overseas Visiting Scholarship while on sabbatical in Cambridge during Lent Term 2005. We thank Angela Huckle and Simon Crowhurst for their assistance in silt size analysis.

National Center for Environmental Prediction (NCEP) Reanalysis data were provided by the National Oceanic and Atmospheric Administration, Office of Atmospheric Research, Earth System Research Laboratory, Physical Science Division (NOAA/OAR/ESRL PSD), Boulder, Colorado, USA, from their web site at <http://www.cdc.noaa.gov>.

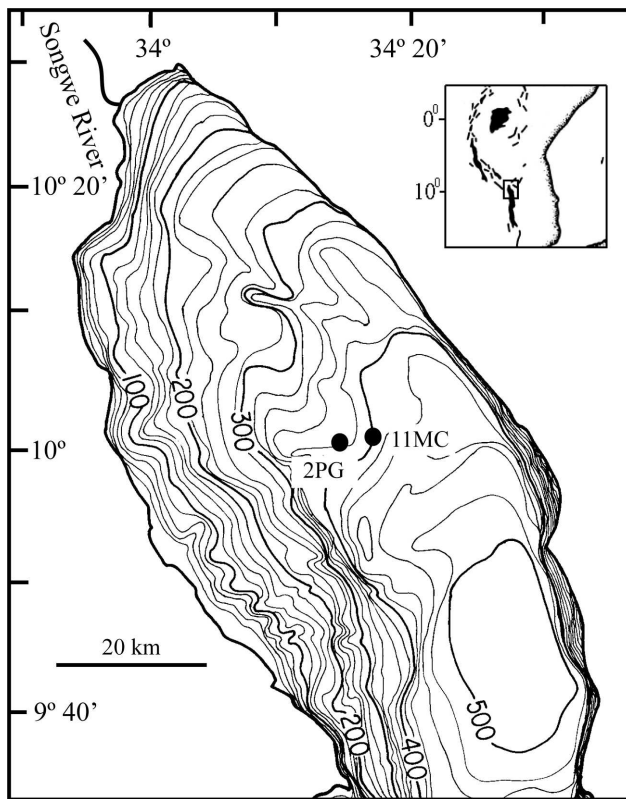


Fig. 1. Location of the core site in northern Lake Malawi. Depth contours are in meters.

11MC, and (2) varve counts coupled with stratigraphic correlations between cores for the entire time interval considered in this study (Johnson et al. 2001; Brown and Johnson 2005; Fig. 2). Varve counts ranged between 4 cm^{-1} and 10 cm^{-1} and averaged $\sim 7 \text{ cm}^{-1}$. Age error based on repeated counts of the same cores by two individuals is ± 0.5 counts per centimeter, or $\pm 7\%$. Thus the age uncertainty of the oldest sediments is no more than ± 50 yr.

A total of 52 sediment horizons were sampled for size analysis at $\sim 2\text{--}3\text{-cm}$ intervals over a sediment depth range of 92 cm, representing the past 650 yr (Table 1). Approximately 0.4 g of freeze-dried sediment was digested in concentrated hydrogen peroxide at 45°C for 2 d to remove organic matter, then it was centrifuged and rinsed in deionized water three times and digested in 1 mol L^{-1} sodium hydroxide (NaOH) at 85°C for 45 min to remove biogenic silica. Previous analyses for biogenic silica in cores from the north basin established that this digestion would remove all diatoms and phytoliths from the sediments, leaving only mineral grains in the silt and sand fraction (Johnson 2002). The digested residue was again rinsed in deionized water and centrifuged three times and then stored in 25 mL of 0.2% Calgon solution until size analysis was undertaken. Microscopic examination of the residues of four randomly selected samples confirmed that the biogenic remains had been removed. While some authigenic minerals might have survived the sediment digestion, microscopic examination of the sediments in these and

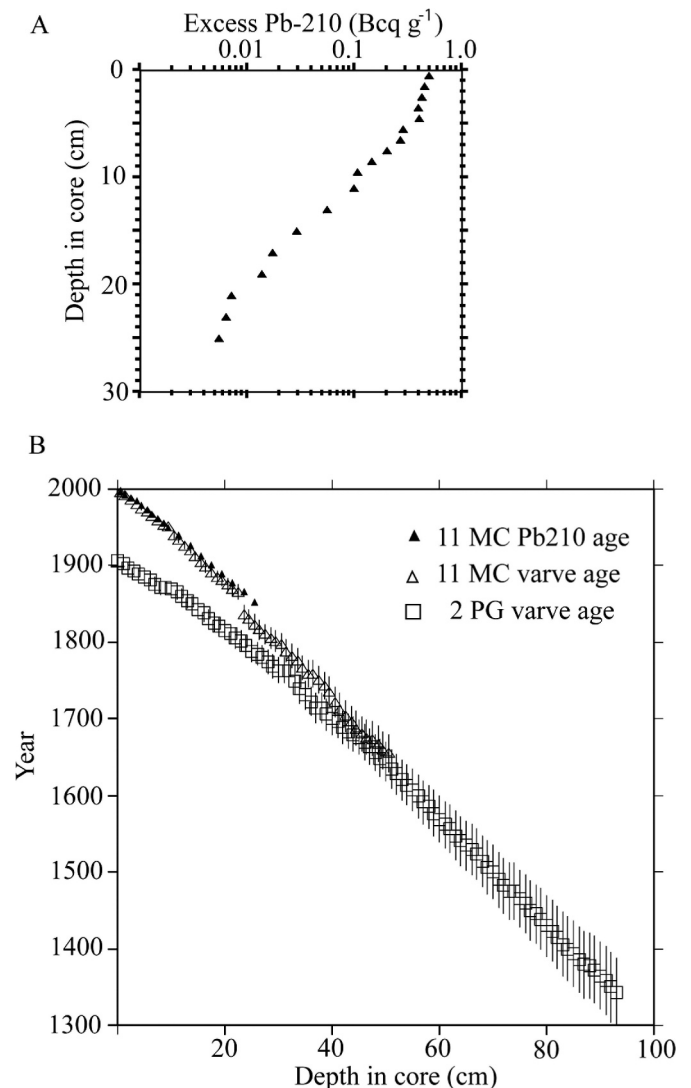


Fig. 2. (A) Excess Pb-210 activity in core 11MC plotted vs. depth (data provided by Paul Wilkinson, Winnipeg). (B) Age models for the two cores, based on Pb-210 in M98-11MC and varve counts. Error bars represent $\pm 7\%$ (see text). The slightly different age–depth profiles for the two cores indicate that 2PG did not re-cover the upper ~ 20 cm of sediment and that the sedimentation rates are slightly different at the two sites.

other cores from the north basin revealed no carbonates and only rare occurrences of vivianite. Angular quartz, feldspar, mica, and heavy minerals derived from the catchment dominate the SS fraction.

Each digested sample was stirred continuously on a vertically rotating turntable for at least 2 d prior to size analysis. Upon removal from the stirring apparatus, a sample was immediately shaken by hand and subsampled by pipette. The subsample was injected into a Multisizer 3 Coulter Counter (Beckman Coulter) fitted with a $200\text{-}\mu\text{m}$ orifice. The Coulter Counter is an electrical-resistance pulse counter that is relatively fast and is a suitable alternative to a device such as a SediGraph, which directly measures settling velocity. The Coulter Counter provides more meaningful results than a laser size analyzer, which yields

Table 1. Analytical results of grain size.

Core	Depth (cm)	Mid- depth (cm)	Age	\overline{SS}	10th	25th	50th	75th	90th
					Percentile				
11MC-A	0.5–1.0	0.75	1,997	16.94	10.60	11.76	15.10	22.34	32.86
11MC-A	2.2–2.7	2.45	1,990	16.55	10.62	11.80	15.00	21.33	30.21
11MC-A	4.1–4.6	4.35	1,979	17.4	10.66	11.99	15.80	23.32	33.6
11MC-A	7.2–7.7	7.45	1,963	17.44	10.63	11.88	15.59	23.91	35.18
11MC-A	9.5–10.0	9.75	1,952	18.07	10.74	12.22	16.25	24.65	36.81
11MC-A	12.0–12.6	12.30	1,931	16.59	10.54	11.54	14.49	21.80	33.01
11MC-A	14.0–14.6	14.30	1,918	16.29	10.52	11.50	14.31	21.1	31.51
11MC-A	16.0–16.6	16.30	1,903	17.59	10.67	11.97	15.65	24.11	35.15
11MC-A	17.5–18.1	17.80	1,893	17.41	10.67	11.97	15.58	23.36	34.26
11MC-A	19.0–19.6	19.30	1,884	16.49	10.59	11.72	14.88	21.74	30.20
11MC-A	20.5–21.1	20.80	1,877	18.12	10.66	12.00	15.96	25.44	38.66
2PG	6.5–7.5	7.00	1,876	17.26	10.58	11.67	15.03	23.54	36.19
2PG	8.9–9.5	9.20	1,871	17.46	10.64	11.92	15.64	23.85	34.55
11MC-A	22.1–22.7	22.40	1,868	17.73	10.66	11.98	15.78	24.23	35.86
2PG	10.0–11.0	10.50	1,867	17.63	10.71	12.15	16.05	23.72	34.34
11MC-A	23.8–24.4	24.10	1,836	16.21	10.55	11.54	14.31	20.63	31.27
11MC-A	25.0–25.6	25.30	1,829	17.21	10.65	11.88	15.33	22.98	34.41
11MC-A	27.0–27.6	27.30	1,815	17.55	10.65	11.96	15.69	24.04	35.22
11MC-A	28.4–29.0	28.70	1,809	16.87	10.58	11.65	14.79	22.20	33.66
11MC-A	29.5–30.1	29.80	1,803	17.68	10.73	12.22	16.20	23.92	33.88
11MC-A	31.0–31.6	31.30	1,794	16.48	10.51	11.47	14.31	21.67	32.91
11MC-A	32.4–33.0	32.70	1,784	17.76	10.63	11.93	15.76	24.88	35.69
11MC-A	33.8–34.6	34.10	1,775	18.88	10.76	12.32	17.08	27.14	39.54
11MC-A	35.8–36.4	36.10	1,759	18.16	10.76	12.33	16.53	24.73	36.20
11MC-A	37.3–37.9	37.60	1,754	17.01	10.59	11.71	15.14	22.79	33.40
11MC-A	38.8–39.5	39.15	1,742	17.79	10.63	11.91	15.78	24.74	36.36
11MC-A	41.0–41.6	41.30	1,719	16.89	10.61	11.79	15.05	22.20	33.03
11MC-A	42.4–43.0	42.70	1,706	16.71	10.57	11.66	14.76	21.6	32.90
2PG	40.0–40.6	40.30	1,699	17.34	10.61	11.80	15.35	23.34	34.78
2PG	42.5–43.5	43.00	1,687	17.38	10.69	12.04	15.74	23.55	33.53
2PG	44.0–44.6	44.30	1,679	17.66	10.62	11.84	15.51	24.48	37.45
11MC-A	46.5–47.0	46.75	1,678	16.37	10.55	11.59	14.63	20.94	31.11
11MC-A	48.0–48.6	48.30	1,672	17.27	10.62	11.82	15.33	23.19	34.29
2PG	46.0–46.6	46.30	1,668	17.90	10.65	11.96	15.84	24.77	37.94
11MC-A	49.5–50.1	49.80	1,661	16.67	10.55	11.60	14.75	21.88	32.68
2PG	48.0–48.6	48.30	1,654	17.90	10.65	12.03	16.11	24.78	36.05
2PG	50.5–51.5	51.00	1,635	17.66	10.65	11.99	15.84	24.13	35.54
2PG	53.0–53.7	53.35	1,618	17.44	10.68	12.03	15.76	23.20	33.71
2PG	56.0–56.6	56.30	1,597	17.10	10.59	11.72	14.99	22.51	35.55
2PG	58–58.7	58.35	1,583	17.86	10.70	12.09	15.93	24.58	36.44
2PG	61.0–61.7	61.35	1,560	16.49	10.55	11.58	14.61	21.62	31.52
2PG	63.0–63.7	63.35	1,545	17.91	10.68	12.04	15.97	24.87	36.48
2PG	66.0–66.7	66.35	1,528	17.38	10.64	11.96	15.9	24.44	35.47
2PG	68.0–68.9	68.45	1,510	17.32	10.62	11.82	15.29	23.32	34.72
2PG	70.8–71.6	71.20	1,488	17.70	10.66	11.96	15.63	24.1	36.62
2PG	73.0–73.7	73.35	1,475	17.43	10.64	11.88	15.46	23.68	35.68
2PG	75.8–76.5	76.10	1,457	17.74	10.64	11.96	15.81	24.55	36.23
2PG	78.0–78.7	78.35	1,443	17.76	10.66	11.95	15.73	24.58	36.69
2PG	81.0–81.6	81.30	1,420	17.72	10.63	11.9	15.62	24.08	36.77
2PG	83.0–83.7	83.35	1,404	17.46	10.58	11.71	15.16	24.02	37.52
2PG	86.0–86.7	86.35	1,383	16.96	10.59	11.69	14.89	22.35	34.09
2PG	88.3–89.4	88.85	1,374	17.47	10.6	11.8	15.38	23.56	36.77
2PG	91.0–91.7	91.35	1,355	17.73	10.71	12.07	15.93	24.47	35.29

distorted size data when platy minerals such as clay and mica are abundant (McCave et al. 2006). Sample concentration in the analyzer cell was kept in the range of 5–15% according to the instrument gauge, which is considered optimal for accuracy. Relative abundance of silt in 64 size

ranges between 10 μm and 63 μm was measured. We calculated the \overline{SS} as well as the 10th, 25th, 50th, 75th, and 90th percentiles in the 10–63 μm range. Each injected sample was analyzed twice, and the average of the two analyses is reported here. Ten of the samples were analyzed in duplicate

(i.e., two separate injections of two analyses each) to assess reproducibility of the pipette withdrawal technique.

The SS wt% was determined in three randomly selected samples by standard pipette analysis, scaled down to the small sample size used in this study. The digested sample, containing clay, silt, and perhaps a few sand grains, was suspended in 0.2% Calgon in a 100-mL centrifuge tube, shaken, and a 5-mL sample was immediately withdrawn by autopipette from mid-depth and transferred to a pre-weighed sample vial for drying and weighing. A second sample was extracted by pipette from a 4-cm depth in the suspension at 8 min after the initial shaking at a laboratory temperature of 17°C, then it was transferred to a preweighed vial for drying and weighing. All silt coarser than 10 μm should have settled below the 4-cm depth by this time (Tanner and Jackson 1947), allowing calculation of SS wt% using the difference in sediment weights between the two withdrawals.

The terrigenous mass accumulation rate (*TMAR*) was calculated from previously published analyses of the cores (Johnson et al. 2001; Barry et al. 2002; Brown and Johnson 2005), using the computational schemes

$$MAR = 10^4(LSR \cdot (1 - \phi) \cdot \rho_{sed}) \quad (1)$$

where *MAR* is the bulk sediment mass accumulation rate ($\text{g m}^{-2} \text{yr}^{-1}$); *LSR* is the linear sedimentation rate derived from the age model (cm yr^{-1}); ϕ is sediment porosity; and ρ_{sed} is dry sediment grain density (g cm^{-3}).

$$TMAR = MAR \cdot (1 - (\%BSi/100) - 2 \cdot (\%TOC))/100 \quad (2)$$

where $\%BSi$ = wt% of biogenic silica (Brown and Johnson 2005); $2 \cdot (\%TOC)$ = wt% total organic matter (Dean 1974); and $\%TOC$ = wt% total organic carbon (Filippi and Talbot 2005).

LSR values were obtained for each centimeter-depth interval, based on the varve counts, and then smoothed by a weighted (1-2-1) 3-point running average. The resultant *TMAR* values were thus smoothed accordingly.

Results

The three pipette analyses yielded values of 15 wt% SS, 26 wt% SS, and 36 wt% SS. All of the samples analyzed in this study appeared to be quite similar in texture, so we concluded that they consisted of approximately one-quarter SS and three-quarters fine silt and clay. The \overline{SS} was remarkably uniform among all samples analyzed, falling in a range of 16.3–18.9 μm with an average value of 17.4 μm and an average standard deviation in the size distribution of 1.6 μm (Table 1). Replicate analyses of \overline{SS} were within $\pm 2.5\%$ of the stated value in 9 of the 10 duplicate samples analyzed, with an average difference based on all 10 duplicates of $\pm 1.9\%$ of the stated value, or $\pm 0.33 \mu\text{m}$. The reproducibility of results in our study is consistent with the error estimate of $\pm 2\%$ of the stated value from an earlier statistical analysis of Coulter Counter results (Bianchi et al. 1999).

Plots of sediment age of \overline{SS} vs. the 10th, 25th, 50th, 75th, and 90th percentiles of the SS size fraction parallel one

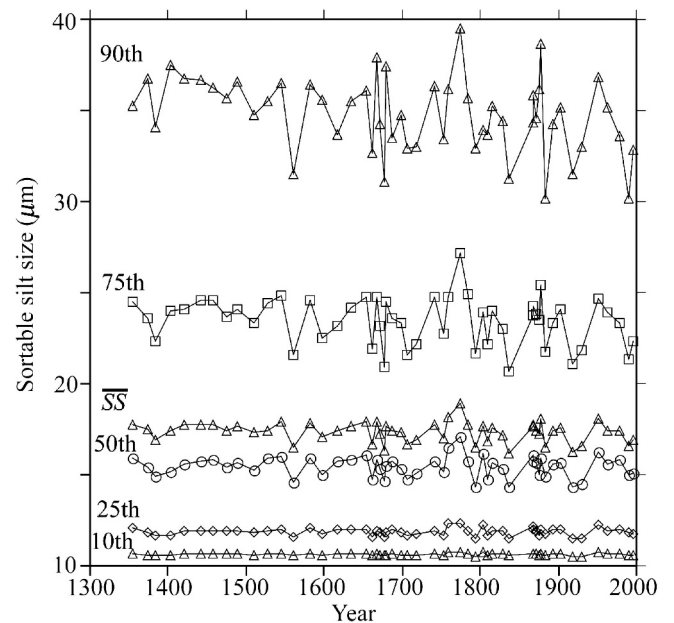


Fig. 3. Profiles of mean sortable-silt size and the designated percentiles of the silt size distribution vs. sediment age.

another, with the 90th percentile exhibiting the greatest range of values (Fig. 3). The \overline{SS} appears to be influenced primarily by the relative abundance of the coarsest fraction of SS, but reflects the size variability in all of the size percentile groups, with the possible exception of the 10th percentile. \overline{SS} also appears to vary with SS wt%, although more pipette analyses would have to be undertaken to determine how robust the relationship is here, but it is generally strong in most data sets (McCave and Hall 2006).

The plot of \overline{SS} vs. sediment age displays some variability in excess of the analytical uncertainty, with an overall trend toward finer \overline{SS} through time (Fig. 4). The \overline{SS} data were smoothed by application of a weighted (1-2-1) 3-point running average. The resultant smoothed curve exhibits symmetrical peaks, with maxima occurring around 1960, 1870, 1780, 1640, 1530, and 1440 (Fig. 4).

The *TMAR* values range between $150 \text{ g m}^{-2} \text{yr}^{-1}$ and $350 \text{ g m}^{-2} \text{yr}^{-1}$ (Fig. 4). The observed range of variability relative to the estimated error bar (i.e., signal-to-noise ratio) is greater for the *TMAR* profile than for the \overline{SS} profile. Overlapping *TMAR* data from the two cores display reasonable agreement, and relatively high peaks in *TMAR* are centered on ~ 1960 , the late 1800's, the early 1600's, the mid-1400's, and then at ~ 100 -yr intervals back to the mid-1200's. Peaks in *TMAR* line up with peaks in \overline{SS} more often than not, but the correlation is neither consistent nor strong (Fig. 4).

Previous site data—Turbid sediment plumes entering Lake Malawi from rivers during the rainy season plunge to a depth of about 40 m, then extend into the basin as interflows, entraining ambient lake water and losing sediment by gravitational settling. McCullough (2006) concluded from a detailed study of the plume dynamics of the Linthipe River in southern Lake Malawi that the sand

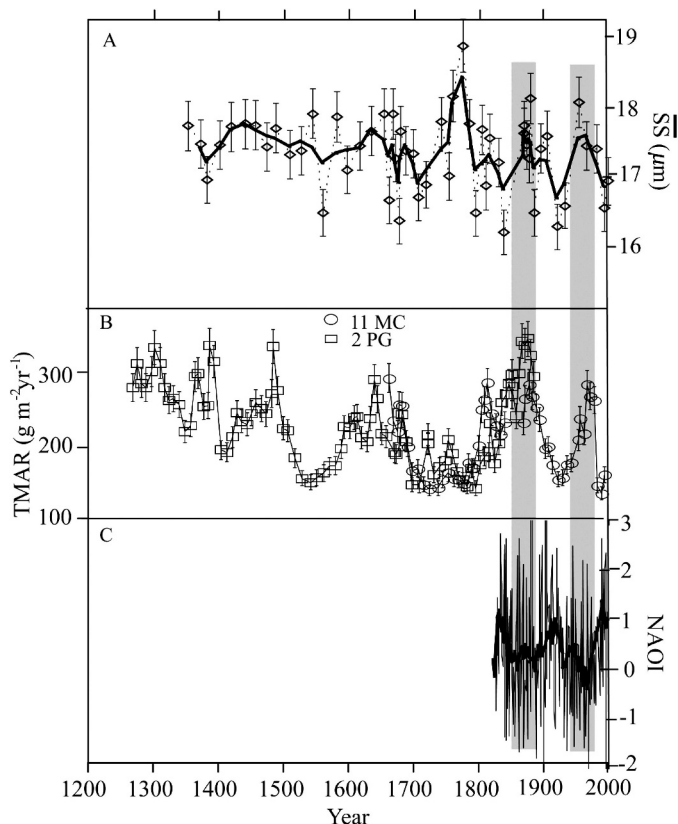


Fig. 4. Plots of (A) \overline{SS} and (B) $TMAR$ for the past 650 yr and (C) the North Atlantic Oscillation Index (NAOI) for December through February (DJF) Index back to 1821 (Hurrell 1995; Jones et al. 1997). The solid line in the upper profile represents a 1-2-1 weighted smoothing of \overline{SS} data. The $TMAR$ data (panel B) have been smoothed in the same manner. The NAOI data have been smoothed by Kaleidograph software (Synergy Software), which uses a Stineman function with geometric weight applied to the data point and $\pm 10\%$ of the data range. Gray shading represents the inverse correlation between the NAOI and the sedimentological parameters, suggesting higher rainfall in the northern Malawi basin during periods of negative NAOI.

and coarse-silt fraction of the fluvial suspended load, which he estimated to be about one third of the total load, is lost by deposition within 600 m of the river mouth. Only fine silt and clay are carried in the intermediate nepheloid layer (INL) along the thermocline (metalimnion) at the base of the surface mixed layer at ~ 40 -m depth. McCullough also reported dilute INLs, in a whole-lake survey, which included the north basin, and concluded that turbid river plumes seldom, if ever, penetrate deeper than the metalimnion.

A conical time-series sediment trap was deployed 100 m above the lake floor (site depth 450 m) in the north basin of Lake Malawi from 1986 to 1989, and samples of the detritus raining to the lake floor were recovered monthly (Pilskaln 2004). The trap effectively captured a seasonal pulse of diatom frustules with other organic matter and fine terrigenous debris settling out of the water column once each year, but did not collect a significant portion of the silt and clay that comprise the dark laminae of the varves accumulating on the lake floor (Pilskaln and Johnson 1991;

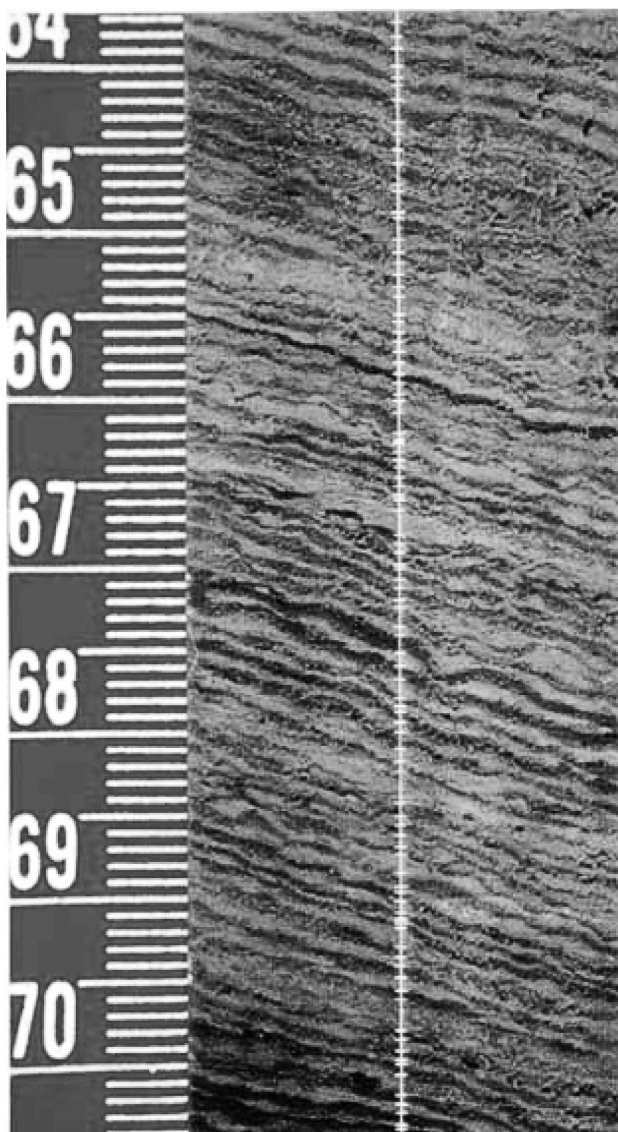


Fig. 5. Photo of varved sediment in core 2PG from northern Lake Malawi. The scale is in centimeters.

Pilskaln 2004). The maximum lithogenic flux observed in the sediment trap was $300 \text{ mg m}^{-2} \text{ d}^{-1}$ and lasted for a month, and the average flux over the 3 yr of measurement was about $10 \text{ g m}^{-2} \text{ yr}^{-1}$ (Pilskaln 2004). The total lithogenic (or terrestrial) mass accumulation rate observed in our cores usually exceeded $200 \text{ g m}^{-2} \text{ yr}^{-1}$ (Fig. 4). The trap was not recovering the vast majority of terrestrial silt and clay delivered to the depositional site, indicating that the SS was being transported to the core site by gravitational flow along the lake floor rather than by fallout from INLs.

The evidence of dating and layer counts indicates that varves of the north basin accumulate consistently each year, with only rare erosional events (Johnson et al. 2001; Barry et al. 2002). Varve thickness, while wavy, always ranges between $1 \text{ mm couplet}^{-1}$ and $2.5 \text{ mm couplet}^{-1}$ (Fig. 5). A lack of obvious erosional unconformities between varves and excellent agreement between varve

counts and Pb-210 geochronology over the past century of deposition (Johnson et al. 2001) indicates that sediment accumulation was uninterrupted by erosional events. There are three homogeneous sediment layers ~1-cm thick (homogenites) interspersed within the varved record of the past 650 yr that have erosional bases on the underlying varves. These homogenites can be correlated among all of our cores from the north basin (Barry 2001) and are interpreted to be distal muddy turbidities (c.f. Dimberline et al. 1990). Apart from these, the underflow plumes of terrigenous clastic material are interpreted to be delivered annually to the offshore basins in the bottom nepheloid layers during or shortly after the rainy season. They deliver, on average, less than one fifth of the amount in a homogenite layer, but over the 650 yr 97% of the material arrives by annual delivery.

Discussion

Silt transport to the offshore basins—The relatively high abundance of SS that we observed must have been transported to the core site along the lake floor. The core site at 350-m depth is some 20 km from the nearest shoreline upslope to the west, and 40 km from the mouth of the Songwe River in the north, which is the major source of sediment into the north basin (Fig. 1). The core site is separated from the closest shoreline to the east by a trough at the base of the eastern border fault (Fig. 1); the catchment area to the east is steep but narrow and is not likely to be a significant source of sediment to the basin floor west of the trough. We envision the annual load of coarse silt delivered by rivers during the rainy season to be deposited temporarily in a few tens of meters of water depth within a kilometer of the river mouth, as observed off the Linthipe River in southern Lake Malawi by McCullough (2006), and perhaps transported by longshore currents in the nearshore region. With the onset of high-wind events at the beginning of the cool season, the seasonal river deposit is resuspended by wave activity and possibly internal wave action on the sharpened pycnocline (Eccles 1974), triggering a sediment gravity flow of the relatively cool surface and thermocline waters that descends basin-ward as a bottom nepheloid layer, i.e., very low-velocity turbidity current (c.f. Halfman and Scholz 1993). Internal wave resuspension may also contribute because numerous lakes have bottom nepheloid layers whose suspension is ascribed to internal wave activity (e.g., Hawley 2004 for Lake Ontario). However, most internal waves are shallower than 100 m in Lake Malawi, and here the resuspension must simply be the initial condition and transport to the core site in 350-m depth driven mainly by gravity.

The slope (S) of the lake floor from the shoreline to a 200-m depth is 1.7×10^{-3} , and from a 200-m depth to the core site at 350 m, $S = 5.4 \times 10^{-3}$. Using the steady uniform flow expression for the speed U of a turbidity current, thickness h , and density ρ_t , under a fluid of density ρ ,

$$U = \left(\frac{g\Delta\rho_t}{\rho} \frac{hS}{C_{D(t+b)}} \right)^{1/2} \quad (3)$$

where $\Delta\rho_t = (\rho_t - \rho)$ and, because the flow has drag on its top and bottom, the drag coefficient includes top and bottom, or $C_{D(t+b)}$. A common value of $C_{D(b)}$ for a deep flow is 0.002 and a rule of thumb is $C_{D(t)} = 0.5C_{D(b)}$ (Middleton 1966), so $C_{D(t+b)} \approx 0.003$. For a flow 10-m thick on a slope of 1.7×10^{-3} in water of $\rho = 1,000 \text{ kg m}^{-3}$ the density difference needed for a flow of $U = 0.1 \text{ m s}^{-1}$ is 0.018 kg m^{-3} and for 0.05 m s^{-1} it is 0.0047 kg m^{-3} . The suspended sediment concentration that yields this density difference is

$$C = \Delta\rho_t / \Delta\rho_s \quad (4)$$

where $\Delta\rho_s$ is $\rho_s - \rho$ and ρ_s is the sediment particle density. This is likely to be a mixture of organic and mineral matter for which values in the range 2,200–2,500 kg m^{-3} are appropriate, given a sediment composition typical for the Malawi north basin: 20 wt% biogenic silica, 4 wt% *TOC*, and the remainder silicate minerals (Filippi and Talbot 2005). For $U = 0.1 \text{ m s}^{-1}$, C is 0.031 kg m^{-3} or 31 g m^{-3} (mg L^{-1}), and for 0.05 m s^{-1} , C is 8 g m^{-3} with $\rho_s = 2,400 \text{ kg m}^{-3}$.

Bagnold suggested that turbidity currents containing particles of a certain size could flow indefinitely if the potential energy lost going down slope generated turbulence intense enough to keep the grains in suspension. The effect of gravity on the grains drags the current down the slope. Bagnold said that the critical particle-settling velocity was $w_s < \bar{U}S$ where \bar{U} was the mean flow of the turbidity current. Pantin (1979) pointed out that this neglects the fact that suspension is an inefficient process—maybe only ~10% efficient—and proposed that $w_s < \bar{U}Se$, where e is suspension efficiency, generally taken to be ~10%. Flows of 5 cm s^{-1} to 10 cm s^{-1} will travel from the delta edge to the 200-m contour in 1 d to 3 d. Such flows will be autosuspending for particles of diameter ~30–40 μm . Once this flow encountered the gentler slope below 200 m it would likely decelerate, but calculations for $S = 5.4 \times 10^{-3}$ yield values of $\Delta\rho_t = 0.057 \text{ kg m}^{-3}$ for $U = 0.1 \text{ m s}^{-1}$ and 0.014 kg m^{-3} for $U = 0.05 \text{ m s}^{-1}$. Corresponding values for C would have to be 98 g m^{-3} and 24 g m^{-3} , respectively, and such a turbid plume would be capable of autosuspending silt of 16–23 μm in diameter. These concentrations are not high, being well below those of a turbid estuary and easily achievable by wave resuspension events (Palanques et al. 2002).

These calculations indicate that silt in the size range we have measured can be transported to the core site by benthic turbid flow. Whether this occurs as a single pulse during the rainy season, or as intermittent flows triggered by resuspension events associated with passing storms several times per year is not known. If the latter is the case, the annual signature of the varves may be due solely to the annual pulse of diatoms superimposed on sporadic cool-season contributions of silt and clay from benthic nepheloid flows.

Paleoclimatic significance of the terrigenous signals—While the *TMAR* and *SS* profiles exhibit alignment of peaks and troughs over the younger part of the record, the relative peak amplitudes of the two parameters vary widely (Fig. 4).

The clear peaks in the *TMAR* record prior to A.D. 1550 are not present (or not aligned) in the *SS* record. We conclude that the environmental factors that most influence the two parameters may show some overlap but are not identical.

TMAR is expected to vary with the sediment yield, i.e., the mechanical denudation rate, of the drainage basin. Sediment yield depends upon a number of factors: drainage basin area and relief, internal storage, mean annual temperature, annual temperature range, and river discharge (Milliman and Syvitski 1992; Hovius 1998; Harrison 2000). Over the study period, we can assume that the physical characteristics of the drainage basin morphology and the regional temperature history have not changed appreciably, and thus variations in *TMAR* are due to changes in river discharge (annual rainfall) alone. The relationship between annual rainfall and sediment yield from a drainage basin is not a simple one. While an increase in rainfall might enhance erosion and sediment transport in rivers, it also promotes soil stabilization through more vigorous growth of vegetation. Moreover, the nature of annual rainfall will affect sediment yield; a year of numerous intense storm events will erode the basin more effectively than a year of relatively gentle, steady rain of similar annual quantity. Finally, changes in agricultural practices may have a severe effect on sediment yield.

Despite these complexities, statistical analyses of global sets of river data have established significant relationships between annual river discharge and sediment yield. These of course have to be considered with caution due to the mathematical consequence of regressing a product (in this case, suspended sediment concentration in a river times river discharge) against a component of the product (river discharge; Hakanson 2006). Nevertheless, there are many examples of a clear linear (in log-log space) relationship between river discharge and sediment flux where the flux is measured independently (Leopold et al. 1964), because rivers are more turbid and discharge is enhanced during periods of heavy rainfall and less turbid during drier conditions. Milliman and Syvitski (1992) analyzed variables for 280 river basins and derived the relationship for an African basin with 1,000-m to 3,000-m relief:

$$Y = aR^b \quad (5)$$

where Y is the sediment yield from the drainage basin ($10^3 \text{ kg km}^{-2} \text{ yr}^{-1}$); a and b are empirical coefficients equal to 20 and 0.65, respectively; R is annual runoff (mm yr^{-1}), and r^2 for the relationship is 0.40.

Hovius (1998) examined more variables for a set of 97 river basins and empirically derived the following relationship:

$$\ln(Y) = -0.416 \ln A + 4.26 \cdot 10^{-4} h_m + 0.15T + 0.095T_r + 0.0015R + 3.585 \quad (6)$$

where A is the drainage basin area (km^2); h_m is the maximum elevation of the drainage basin (m); T is the mean annual temperature in the basin ($^{\circ}\text{C}$); and T_r is the annual temperature range ($^{\circ}\text{C}$).

Over the past 650 yr, T has varied mostly between 23.5°C and 26.5°C (Powers 2005), corresponding to a range of 305–

$480 \times 10^3 \text{ kg km}^{-2} \text{ yr}^{-1}$ in predicted values of sediment yield for the Songwe River basin if all other factors are held constant. By comparison, if R varies between 280 mm yr^{-1} and 840 mm yr^{-1} ($\pm 50\%$ of its measured value in 1997–1998), the range of values predicted for Songwe sediment yield, holding all other variables in Eq. 6 constant, is $290\text{--}680 \times 10^3 \text{ kg km}^{-2} \text{ yr}^{-1}$. Thus mean annual temperature appears to have one third as much effect on sediment yield as does mean annual rainfall or river discharge. The Hovius equation could be rewritten:

$$\ln Y = C + 0.15T + 0.0015R \quad (7)$$

where C is a constant and the other variables in Eq. 6 are assumed to not have varied significantly over the 700 yr encompassed in this study.

Harrison (2000) re-examined the data set of Hovius (1998) and arrived at a similar equation to Eq. 6, but incorporated terms of mean maximum monthly river discharge instead of mean annual monthly river discharge, and basin length and mean slope instead of A and h_m in Eq. 6. Assuming constant conditions of basin morphology and annual temperature range, this yields an equation much like Eq. 7:

$$\ln Y = D + 0.151T + 0.00075R_m \quad (8)$$

where D is a constant and R_m is the maximum monthly discharge in mm yr^{-1} and has been assigned a value five times the mean annual discharge for the Lake Malawi rivers, based on data from (Bootsma et al. 2003).

Thus in each of these statistical analyses of large sets of river data, sediment yield, or annual erosion rate, was found to vary directly, albeit nonlinearly, with temperature and annual river discharge or, by inference, annual rainfall. The mean grain size of the whole sediment load delivered to the lake would also be expected to rise as discharge rises because of higher flow velocities and shear stresses, but this increase would be conferred by incorporation of more sand into the mixture, not by a change in *SS*. The mean would not be expected to increase with temperature. On the contrary, an increase in temperature hastens chemical weathering processes, thereby increasing sediment yield from a drainage basin, but at the same time might be expected to decrease mean mud size by increasing clay and fine silt production.

A comparison of predicted sediment yields by Eqs. 5, 7, and 8 with measured yields of three rivers in the north basin of Lake Malawi in 1997 (Table 2) suggests that the empirical equations of Hovius (1998) and Harrison (2000) are better predictors of yield than the equation of Milliman and Syvitski (1992).

While *TMAR* might respond to rainfall, it is less obvious that *SS* would be similarly controlled because that would imply size selection in the entrainment of fine cohesive material into the river channel. Experimental data suggest that, because of cohesion, such size selection is unlikely (Winterwerp and Van Kesteren 2004; Law et al. in press). *SS* indicates the flow speed of the depositing suspension, and this is more likely to be determined by the intensity of sediment resuspension in coastal water during the dry,

Table 2. Drainage basin characteristics, runoff, and sediment yield for three rivers in the northern catchment of Lake Malawi in 1997. Maximum elevation values taken from topographic map in Hamblin et al. (2003) and river drainage basin area (DBA), runoff, and sediment yield from Hecky et al. (2003). Predicted sediment yields in metric tons $\text{km}^{-2} \text{yr}^{-1}$ are from Eq. 5 from Milliman and Syvitski (1992; M&S), Eq. 6 from Hovius (1998), and Eq. 8 modified from Harrison (2000).

River	Drainage basin area (km^2)	Max. elev. (m)	Mean temp. ($^{\circ}\text{C}$)	Temp. range ($^{\circ}\text{C}$)	Ann. runoff (mm yr^{-1})	Mean slope (m km^{-1})	Basin length (km)	Max. monthly runoff (mm yr^{-1})	M&S predicted ($\text{t km}^{-2} \text{yr}^{-1}$)	Hovius predicted ($\text{t km}^{-2} \text{yr}^{-1}$)	Harrison predicted ($\text{t km}^{-2} \text{yr}^{-1}$)	Hecky observed ($\text{t km}^{-2} \text{yr}^{-1}$)
Songwe	4,280	1,600	26	6	559	24	130	2,800	7,267	444	1,276	661
Lufia	1,440	800	26	6	158	21	70	790	2,054	272	172	141
North Rukuru	1,970	1,200	26	6	244	27	90	1,220	3,172	322	365	145

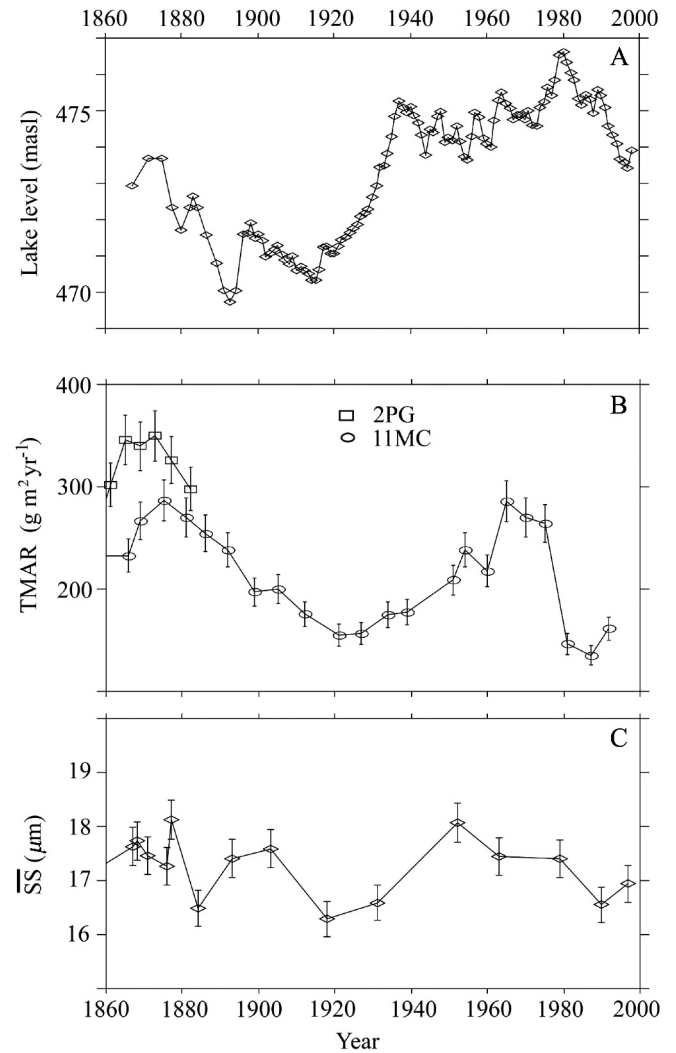


Fig. 6. (A) Historical record of lake level back to 1896, and estimated from explorers' records prior to that. (B) $TMAR$ plots for cores 11MC and 2PG. (C) Mean sortable-silt size vs. age.

windy conditions of austral winter. Intense winds would entrain more sediment than less energetic weather events, with greater potential for generating relatively thick and dense turbidity currents capable of transporting coarser material farther offshore (*see Eq. 3*).

We tested the ties of \overline{SS} and $TMAR$ to rainfall by comparing their values with the level of Lake Malawi over the past 140 yr of measurement. The surface elevation of the lake varied by 6 m over that time, and it was actually a closed basin in the first three decades of the twentieth century, when its level dropped below the sill of the outflowing Shire River. A beach ridge formed at the outlet, effectively damming outflow until lake level rose in the 1930's (Pike and Rimmington 1965). The $TMAR$ curve roughly tracks lake level, while the \overline{SS} curve displays less correlation (Fig. 6). Values of $TMAR$ were relatively high in the late 1800's prior to the fall in lake level and then fell to minimum values around 1920 when the lake was a closed basin. As lake level rose in the 1930's, values of $TMAR$ rose as well, although with a substantial lag behind lake level

(Fig. 6). Peak values of $TMAR$ around 1870–1880 (Fig. 4) coincide with coral records exhibiting high sea surface temperatures (SSTs) around 1878 from the western and eastern equatorial Indian Ocean (Charles et al. 1991; Cole et al. 2000), a year of a major El Niño Southern Oscillation (ENSO) event and a year of very heavy rains in East Africa (Nicholson 1999). The peak value of $TMAR$ in the early 1960's may reflect the unusually intense rainfall that affected much of tropical East Africa in late 1961, an event tied to an SST gradient reversal in the equatorial Indian Ocean (Flohn 1987; Conway 2002).

In data over the last 100 yr, there is a correlation between \overline{SS} and $TMAR$ and the North Atlantic Oscillation Index (NAOI; Hurrell 1995; Jones et al. 1997) which was negative from 1865 to 1905, positive from 1905 to 1930, negative from 1930 to 1970, and positive from 1970 to 2000 (Fig. 4). Positive NAOI corresponds to low $TMAR$ and \overline{SS} . This is consistent with reported correlation between negative NAOI and high rainfall in East Africa between the equator and 16°S (McHugh and Rogers 2001). The correlation may be related to control of the intertropical convergence zone (ITCZ) position by the pressure field expressed in the NAOI, or to the effect of ENSO on the Northern Hemisphere annular mode and North Atlantic Oscillation (NAO; e.g., Quadrelli and Wallace 2002). Several authors have noted and examined a correlation between indices of ENSO and NAO.

Values of $TMAR$ and \overline{SS} dropped in the latter half of the 20th century, well in advance of a minor but prolonged drop in lake level beginning around 1980. The drop in $TMAR$ in the top three samples, representing the top 4 cm of sediment, reflects the much higher porosity of this part of the core (~0.96 vs. 0.93 immediately below 4 cm). Such a relatively small change in porosity results in major changes (>40%) in $(1 - \phi)$ and calculated value of $TMAR$ in Eq. (1).

Divergence in the $TMAR$ and \overline{SS} profiles, most notably prior to the 19th century, reflects the disparate climatic factors that affect the two sedimentary parameters. $TMAR$ is most affected by rainfall and temperature, whereas \overline{SS} is probably most influenced by sediment resuspension in coastal water by surface and internal wave energy, a function of southerly wind intensity and duration. Unfortunately, continuous wind data in the region are not available for a sufficient number of years to test this hypothesis. Alternatively we compare \overline{SS} to National Center for Environmental Prediction (NCEP) Reanalysis (Kalnay et al. 1996) of meridional winds over the northern sector of Lake Malawi for 1948–2000. A crude correlation exists, but the tie is understandably weak (Fig. 7). Mean monthly wind data will not capture the intensity of individual events, and the specific locale of sediment resuspension, as well as the amount available for resuspension, will undoubtedly vary with any given storm. We observed no apparent correlation between NCEP meridional winds over northern Lake Malawi and the NAOI.

The size distribution of SS (10–64- μm diameter) deposited in varved, diatomaceous silty clays in the north basin of Lake Malawi has been remarkably uniform over the past 650 yr, with mean size (\overline{SS}) ranging between ~16 μm and 18 μm . Results from earlier studies on river plume dynamics

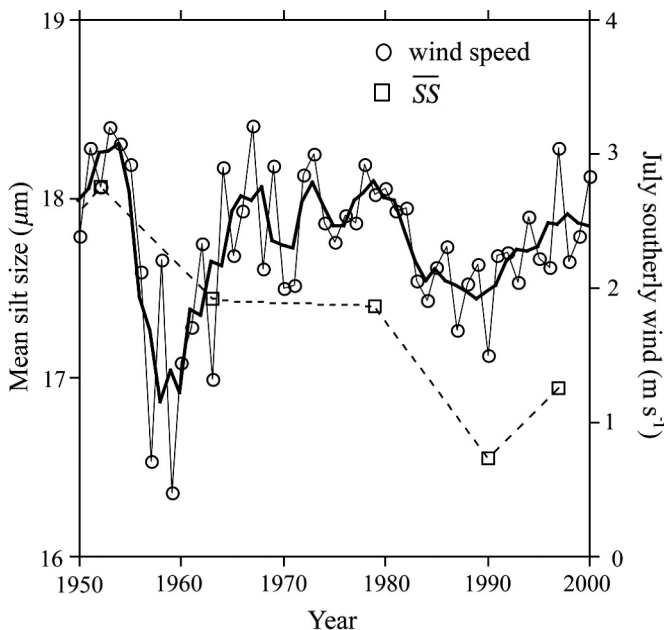


Fig. 7. Mean sortable-silt size and mean July meridional wind speed from NCEP Reanalysis for the northern basin of Lake Malawi for the period 1950–2000. The solid line is a 1-1-1 smoothing of the wind speed data.

(McCullough 2006) and with conical time series sediment traps (Pilska 2004) in Lake Malawi, coupled with our data, indicate that most of the terrigenous sediment arrives in the offshore basin in benthic nepheloid plumes migrating down a slope with sufficient turbulence to maintain coarse silt in suspension, yet are slow enough to allow deposition along the flow path. Profiles of \overline{SS} and of $TMAR$ covary over much, but not all, of the 650-yr interval that we investigated. The profile of $TMAR$ roughly tracks the lake-level curve of the past 140 yr, and displays a rather striking inverse correlation with the results of the past 180 yr. This is consistent with the results of McHugh and Rogers (2001), who reported an inverse relationship between NAO index and annual rainfall in East Africa between the equator and 16°S. However, East African rainfall is known to be influenced primarily by ENSO events and SST patterns in the Indian Ocean (Goddard and Graham 1999). Our results add credence to the suspected interdependence between NAO and ENSO. While the signal of \overline{SS} is relatively weak, its correlation to the meridional wind field of Lake Malawi, generated by NCEP Reanalysis, indicates that \overline{SS} may be a valuable proxy of past environmental conditions in the Malawi basin. However, our understanding of precisely how coarse silt is delivered to the offshore basins, that is, by a single major nepheloid event each year shortly after the rainy season, or as a series of nepheloid events associated with passing storms throughout the year, needs to be resolved before the paleoclimatic significance of the \overline{SS} signal can be fully exploited.

References

- BARRY, S. L. 2001. Stratigraphic correlation and high-resolution geochronology of varved sediments from Lake Malawi, East Africa. M.S. thesis, Univ. of Minnesota.

- , M. L. FILIPPI, M. R. TALBOT, AND T. C. JOHNSON. 2002. A 20,000-yr sedimentological record from Lake Malawi, East Africa: The late-Pleistocene/Holocene transition in the southern tropics, p. 369–392. *In* E. O. Odada and D. O. Olago [eds.], *The East African Great Lakes: Limnology, palaeoclimatology, and biodiversity*. Kluwer.
- BIANCHI, G. G., I. R. HALL, I. N. McCAVE, AND L. JOSEPH. 1999. Measurement of the sortable silt current speed proxy using the Sedigraph 5100 and Coulter Multisizer II: Precision and accuracy. *Sedimentology* **46**: 1001–1014.
- BOOTSMA, H. A., R. E. HECKY, T. C. JOHNSON, H. KLING, AND J. MWITA. 2003. Inputs, outputs, and internal cycling of silica in a large, tropical lake. *J. Great Lakes Res.* **29**: 121–138.
- BROWN, E. T., AND T. C. JOHNSON. 2005. Coherence between tropical East African and South American records of the Little Ice Age. *G3* **6**: Q12005, doi:10.29/2005GC000959.
- CHARLES, C. D., D. E. HUNTER, AND R. G. FAIRBANKS. 1991. Interaction between the ENSO and the Asian monsoon in a coral record of tropical climate. *Science* **277**: 925–928.
- COLE, J. E., R. B. DUNBAR, T. R. McCLANAHAN, AND N. A. MUTHIGA. 2000. Tropical Pacific forcing of decadal SST variability in the western Indian Ocean over the past two centuries. *Science* **287**: 617–619.
- CONWAY, D. 2002. Extreme rainfall events and lake level changes in East Africa: Recent events and historical precedents, p. 63–92. *In* E. O. Odada and D. O. Olago [eds.], *The East African Great Lakes: Limnology, palaeolimnology and biodiversity*. Kluwer.
- DEAN, W. E. 1974. Determination of carbonate minerals and organic matter in calcareous sediments and sedimentary rocks by loss on ignition: Comparison with other methods. *J. Sediment. Petrol.* **44**: 242–248.
- DIMBERLINE, A. J., A. BELL, AND N. H. WOODCOCK. 1990. A laminated hemipelagic facies from the Wenlock and Ludlow of the Welsh Basin. *J. Geol. Soc. Lond.* **147**: 693–701.
- ECCLES, D. H. 1974. An outline of the physical limnology of Lake Malawi (Lake Nyasa). *Limnol. Oceanogr.* **19**: 730–742.
- FILIPPI, M. L., AND M. K. TALBOT. 2005. The palaeolimnology of northern Lake Malawi over the last 25 ka based upon the elemental and stable isotopic composition of sedimentary organic matter. *Quat. Sci. Rev.* **24**: 1303–1328.
- FLOHN, H. 1987. East African rains of 1961–62 and the abrupt change of the White Nile discharge. *Palaeocol. Afr.* **18**: 3–18.
- GODDARD, L., AND N. E. GRAHAM. 1999. Importance of the Indian Ocean for simulating rainfall anomalies over eastern and southern Africa. *J. Geophys. Res.* **104**: 19099–19116.
- HAKANSON, L. 2006. Suspended particulate matter in lakes, rivers and marine systems., Blackburn.
- , AND A. KALLSTROM. 1978. An equation of state for biologically active late sediments and its implications for interpretations of sediment data. *Sedimentology* **25**: 205–226.
- HALFMAN, J. D., AND C. A. SCHOLZ. 1993. Suspended sediments in Lake Malawi, Africa: A reconnaissance study. *J. Great Lakes Res.* **19**: 499–511.
- HARRISON, C. G. A. 2000. What factors control mechanical erosion rates? *International J. Earth Sci.* **88**: 752–763.
- HAWLEY, N. 2004. Response of the benthic nepheloid layer to near-inertial internal waves in southern Lake Michigan. *J. Geophys. Res. Oceans* **109**(C4): C04007, doi: 10.29/2003JC002128.
- HUVIUS, N. 1998. Controls on sediment supply by large rivers. *SEPM Spec. Pub.* **59**: 3–16.
- HURRELL, J. W. 1995. Decadal trends in the North Atlantic Oscillation and relationships to regional temperature and precipitation. *Science* **269**: 676–679.
- JOHNSON, T. C. 1996. Sedimentary processes and signals of past climatic change in the large lakes of the East African Rift Valley, p. 367–412. *In* T. C. Johnson and E. O. Odada [eds.], *The limnology, climatology, and paleoclimatology of the East African lakes*. Gordon and Breach.
- . 2002. Biogenic silica profiles in the sediments of large tropical lakes: examples from East Africa, p. 247–255. *In* R. W. Renaut and G. M. Ashley [eds.], *Sedimentation in continental rifts*. Soc. Econ. Paleont. Mineralog.
- , S. L. BARRY, Y. CHAN, AND P. WILKINSON. 2001. Decadal record of climate variability spanning the last 700 yr in the southern tropics of East Africa. *Geology* **29**: 83–86.
- JONES, P. D., T. JONSSON, AND D. WHEELER. 1997. Extensions to the North Atlantic Oscillation using early instrumental pressure observations from Gibraltar and South West Iceland. *Int. J. Clim.* **17**: 1433–1450.
- KALNAY, E., AND OTHERS. 1996. The NCEP/NCAR 40-year reanalysis project. *Bull. Am. Meteorol. Soc.* **77**: 437–470.
- LAW, B. A., P. S. HILL, T. G. MILLIGAN, K. J. CURRAN, P. L. WIBERG, AND R. A. WHEATCROFT. In press. Size sorting of fine-grained sediments during erosion: Results from the western Gulf of Lions. *Cont. Shelf Res.*
- LEOPOLD, L. B., M. G. WOLMAN, AND J. P. MILLER. 1964. Fluvial processes in geomorphology. Freeman.
- McCAVE, I. N., AND I. R. HALL. 2006. Size sorting in marine muds: Processes, pitfalls, and prospects for palaeoflow-speed proxies. *Geochem. Geophys. Geosyst.* **7**: Q10N05, doi:10.1029/2006GC001284.
- , ———, AND G. G. BIANCHI. 2006. Laser versus settling velocity differences in silt grainsize measurements: Estimation of palaeocurrent vigour. *Sedimentology* **53**: 919–928.
- McCULLOUGH, G. K. 2006. Circulation of terrestrial runoff and its suspended load in a large tropical lake: A study of processes and effects near the mouth of the Linthipe River in Lake Malawi. Ph.D. thesis, Univ. of Manitoba.
- McHUGH, M. J., AND J. C. ROGERS. 2001. North Atlantic Oscillation influence on precipitation variability around the southeast African convergence zone. *J. Clim.* **14**: 3631–3642.
- MIDDLETON, G. V. 1966. Experiments on density and turbidity currents, II. Uniform flow of density currents. *Can. J. Earth Sci.* **3**: 627–637.
- MILLIMAN, J. D., AND J. SYVITSKI. 1992. Geomorphic/tectonic control of sediment discharge to the ocean: The importance of small mountainous rivers. *J. Geol.* **100**: 525–544.
- NICHOLSON, H. F. 1999. Historical and modern fluctuations of lakes Tanganyika and Rukwa and their relationship to rainfall variability. *Clim. Change* **41**: 53–71.
- PALANQUES, A., AND OTHERS. 2002. Near-bottom suspended sediment fluxes on the microtidal low-energy Ebro continental shelf (NW Mediterranean). *Cont. Shelf Res.* **22**: 285–303.
- PANTIN, H. M. 1979. Interaction between velocity and effective density in turbidity flow: phase-plane analysis, with criteria for autosuspension. *Mar. Geol.* **31**: 59–99.
- PIKE, J. G., AND G. T. RIMMINGTON. 1965. *Malawi. A geographical study*. Oxford.
- PILSKALN, C. H. 2004. Seasonal and interannual particle export in an African rift valley lake: A 5-yr record from Lake Malawi, southern East Africa. *Limnol. Oceanogr.* **49**: 964–977.
- , AND T. C. JOHNSON. 1991. Seasonal signals in Lake Malawi sediments. *Limnol. Oceanogr.* **36**: 544–557.
- POWERS, L. A. 2005. Calibration and application of a new paleo-temperature tool in lacustrine systems: TEX86 for continental paleoclimate reconstruction. Ph.D. thesis, Univ. of Minnesota.

- QUADRELLI, R., AND J. M. WALLACE. 2002. Dependence of the structure of the Northern Hemisphere annular mode on the polarity of ENSO. *Geophys. Res. Lett.* **29**: 2132, doi:10.1029/2002GL015807.
- ROWAN, D. J., J. KALFF, AND J. B. RASMUSSEN. 1992. Estimating the mud deposition boundary depth in lakes from wave theory. *Can. J. Earth Sci.* **49**: 2490–2497.
- STANLEY, D. J., AND C. M. WEAR. 1978. The mud line: an erosion-deposition boundary on the upper continental slope. *Mar. Geol.* **28**: 19–29.
- TALBOT, M. R. 1988. The origins of lacustrine oil source rocks: evidence from the lakes of tropical Africa, p. 29–43. *In* A. J. Fleet, K. Kelts and M. R. Talbot [eds.], *Lacustrine petroleum source rocks*. Geological Society Special Publication.
- TANNER, C. B., AND M. L. JACKSON. 1947. Nomographs of sedimentation times for soil particles under gravity or centrifugal acceleration. *Proc. Soil Science Soc. Amer.* **12**: 60–65.
- WINTERWERP, J. C., AND W. G. M. VAN KESTEREN. 2004. *Introduction to the physics of cohesive sediment in the marine environment*. Elsevier.

Received: 16 October 2007
Accepted: 23 January 2008
Amended: 12 March 2008